Sedimentology (2000) **47**, 1181–1197

Sedimentary processes in the Selvage sediment-wave field, NE Atlantic: new insights into the formation of sediment waves by turbidity currents

RUSSELL B. WYNN*, PHILIP P. E. WEAVER*, GEMMA ERCILLA‡, DORRIK A. V. STOW† and DOUGLAS G. MASSON*

**Challenger Division and †School of Ocean and Earth Science, Southampton Oceanography Centre, European Way, Southampton, Hampshire SO14 3ZH, UK (E-mail: rbw1@soc.soton.ac.uk)*

‡Instituto Ciencias del Mar, CSIC, Paseo Juan de Borbon s/n, 08039 Barcelona, Spain

ABSTRACT

An integrated geophysical and sedimentological investigation of the Selvage sediment-wave field has revealed that the sediment waves are formed beneath unconfined turbidity currents. The sediment waves occur on the lower continental rise and display wavelengths of up to 1 km and wave heights of up to 6 m. Wave sediments consist of interbedded turbidites and pelagic/hemipelagic marls and oozes. Nannofossil-based dating of the sediments indicates a bulk sedimentation rate of 2·4 cm 1000 years^{-1}, and the waves are migrating upslope at a rate of 0·28 m 1000 years^{-1}. Sediment provenance studies reveal that the turbidity currents maintaining the waves are largely sourced from volcanic islands to the south. Investigation of existing models for sediment-wave formation leads to the conclusion that the Selvage sediment waves form as giant antidunes. Simple numerical modelling reveals that turbidity currents crossing the wave field have internal Froude numbers of 0·5–1·9, which is very close to the antidune existence limits. Depositional flow velocities range from <6 to 125 cm^{-1}. There is a rapid increase in wavelength and flow thickness in the upper 10 km of the wave field, which is unexpected, as the slope angle remains relatively constant. This anomaly is possibly linked to a topographic obstacle just upslope of the sediment waves. Flows passing over the obstacle may undergo a hydraulic jump at its boundary, leading to an increase in flow thickness. In the lower 15 km of the wave field, flow thickness decreases downslope by 60%, which is comparable with results obtained for other unconfined turbidity currents undergoing flow expansion.

Keywords Froude number, sediment waves, turbidity currents.

INTRODUCTION

Deep-water sediment waves are a type of large-scale depositional bedform that may be generated beneath alongslope-flowing bottom currents or downslope-flowing turbidity currents. Sediment waves have been referred to previously as gravel waves (Shor *et al.*, 1990), sand waves (Kenyon & Belderson, 1973), mud waves (e.g. Lewis *et al.*, 1998), lower continental rise hills (Rona, 1969), abyssal antidunes (Fox *et al.*, 1968), giant ripples (Ewing *et al.*, 1968) and depositional ridges (Johnson & Schneider, 1969). Although most of the recently published literature correctly refers to them as sediment waves, this variety of terms can still create confusion. In the present study, a sediment wave is defined as a large-scale (generally tens of metres to a few kilometres wavelength and several metres high), sinusoidal, depositional bedform that is generated beneath a current flowing on the sea floor. Sediment waves may be composed of sediment of any grain size

from gravel to mud. It is recommended that the basic definition of 'coarse-grained sediment waves' (sand and gravel dominated) and 'fine-grained sediment waves' (mud dominated) is applied to future studies to avoid further confusion.

Turbidity-current (TC) sediment waves generally occur on the backslopes of channel levées (Damuth, 1979; Normark *et al.*, 1980; Carter *et al.*, 1990; Piper & Savoye, 1993; Droz *et al.*, 1996; McCave & Carter, 1997; Lewis *et al.*, 1998; Nakajima *et al.*, 1998; Piper *et al.*, 1999) and in turbidity-current channels (Malinverno *et al.*, 1988; Shor *et al.*, 1990; Kidd *et al.*, 1998; Lewis *et al.*, 1998; Morris *et al.*, 1998; Wynn *et al.*, 2000a). TC sediment waves have also been described from submarine fans (Kenyon *et al.*, 1995; Howe, 1996) and open slopes flanking volcanic islands (Wynn *et al.*, 2000a). TC sediment waves display wavelengths of up to 6 km and wave heights of up to 70 m, commonly show a downslope decrease in dimensions (Table 1) and typically occur on slopes of <2°. Wave crests are aligned parallel or subparallel to the slope and are therefore perpendicular to TC flow. Cores taken through sediment-wave sequences on levées and open slopes contain interbedded thin turbidites and pelagic/hemipelagic sediments. Sediment waves within channels are generally dominated by coarse-grained turbidites rich in sand and gravel.

Although TC sediment waves display very similar characteristics to sediment waves formed beneath bottom currents, previous hydrodynamic interpretations of TC sediment waves have favoured the 'antidune' model, suggesting that the waves form as giant antidunes beneath flows with a Froude number close to unity (Normark *et al.*, 1980; Howe, 1996; McCave & Carter, 1997; Wynn *et al.*, 2000a).

In the present study, a sediment-wave field on the lower continental rise north of the volcanic Selvage and Canary Islands (Fig. 1) is described using a data set containing high-resolution TOPAS (TOpographic PArametric Sonar) profiles and a single giant piston core. The wave field is referred to as the Selvage sediment-wave field because of its close proximity to the Selvage Islands. Nannofossil-based dating of the sediments has allowed sedimentation and wave migration rates to be calculated. The principal objectives of the present study are to: (1) interpret the wave-forming processes in the Selvage wave field; and (2) present some new insights into the formation of sediment waves by turbidity

Table 1. Examples of sediment-wave fields formed beneath unconfined turbidity currents.

Wave field setting	Max. WH (m)	Max. WL (km)	Slope angle (°)	Comments	Reference
Selvage wave field: lower continental rise	5	1·1	0·13–0·22	WL + WH decrease downslope, crests parallel to slope	This study
La Palma wave field: continental slope/rise	70	2·4	0·4–1·8	WL + WH decrease downslope, crests sinuous and parallel to slope	Wynn *et al.* (2000a)
Bounty Channel: levée backslope	17	6	0·3–0·7	WL + WH decrease downslope, crests parallel to slope	Carter *et al.* (1990)
Toyama Channel: levée backslope	70	3	0·4–1·4	WL + WH decrease downslope, crests sinuous and parallel to slope	Nakajima *et al.* (1998)
Hikurangi Channel: levée backslope	15	3	?	WL + WH decrease downslope, crests subparallel to slope	Lewis *et al.* (1998)
Monterey Fan: levée backslope	37	2·1	0·8	WL + WH decrease downslope, sinuous crests subparallel to slope	Normark *et al.* (1980)
Hueneme Fan: levée backslope	10	0·6	0·8	WL + WH decrease downslope	Piper *et al.* (1999)
Var Fan: levée backslope	50	7	0·5–1·7	WL + WH increase downslope (slope steepens), crests oblique to slope	Piper & Savoye (1993)
Barra Fan: distal fan slope	5	1·75	?	Crests possibly oblique to slope	Howe (1996)

Note that all wave fields occur on slopes of 0·1–1·7°, wave dimensions generally decrease downslope and wave crests are aligned parallel/subparallel to the slope.
WH, wave height; WL, wavelength.

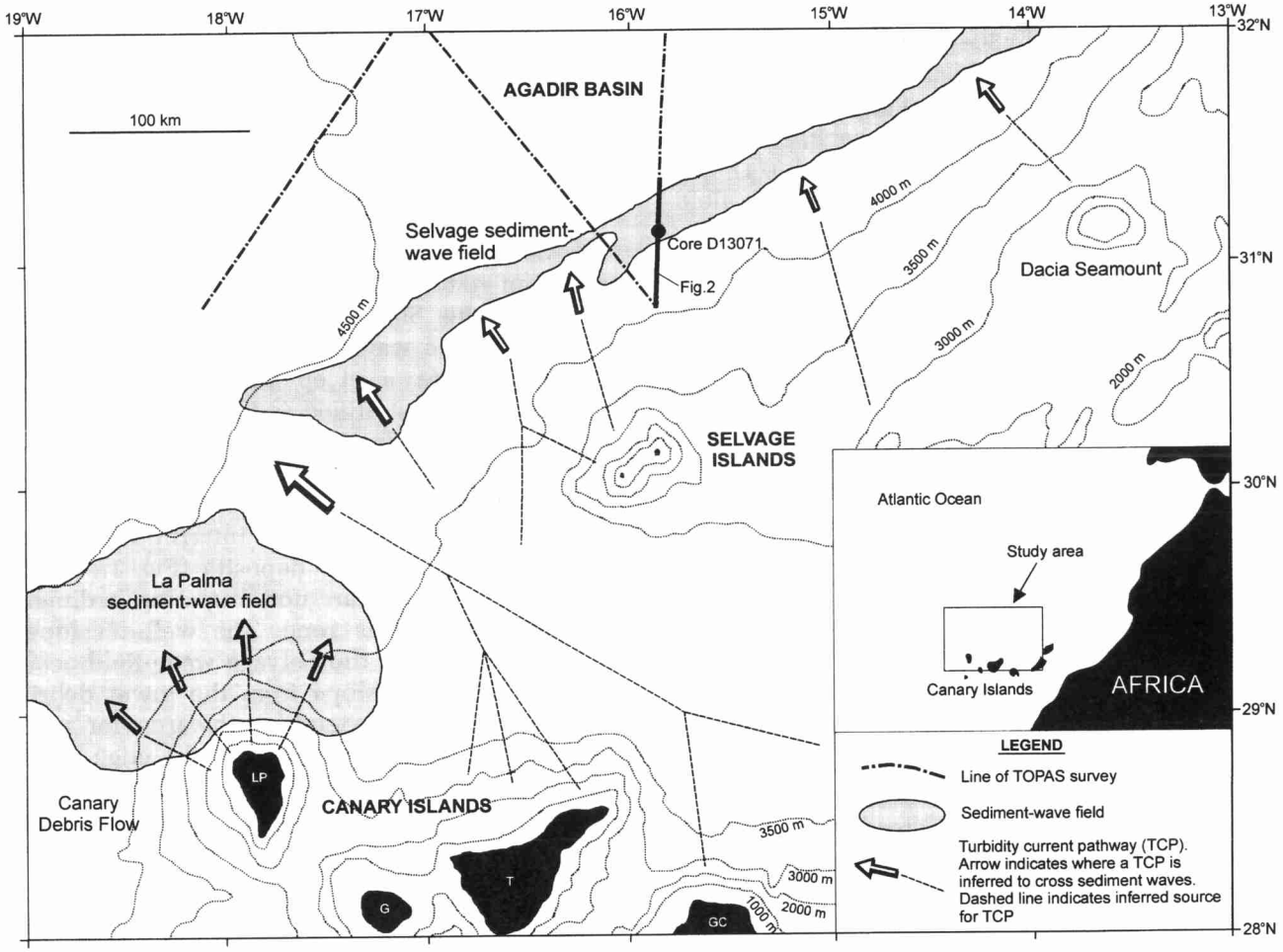

Fig. 1. Location map showing the position of sediment-wave fields and TC pathways on the continental slope and rise north of the Canary Islands. The location of TOPAS lines and core D13071 are also indicated. Island names are as follows: LP, La Palma; G, Gomera; T, Tenerife; GC, Gran Canaria. The boundary of the Selvage sediment-wave field has been modified from Jacobi *et al.* (1975). The boundary of the La Palma sediment-wave field is based on a map by Wynn *et al.* (2000a).

currents, based on the new data and previously published examples.

PREVIOUS WORK

Sediment waves on the Moroccan continental rise north of the Canary Islands were first recognized on 3·5-kHz profiles by Jacobi *et al.* (1975), who tentatively concluded that bottom currents were primarily responsible for wave formation, but that turbidity currents might also have been influential in wave formation and distribution. A more recent study has been undertaken on the La Palma sediment-wave field, offshore of the western Canary Islands (Wynn *et al.*, 2000a). Wynn *et al.* (2000a) used a high-quality integrated data set to reveal sediment-wave morphology in the La Palma sediment-wave field and concluded that the waves were formed beneath unconfined turbidity currents sourced from the island flanks (Fig. 1).

DATA COLLECTION

About 600 km of ultrahigh-resolution seismic profiles was obtained using the TOPAS system during cruise MAYC-95. The TOPAS system is a hull-mounted seabed and sub-bottom echo sounder based on a parametric acoustic array, which operates using non-linear acoustic properties of the water (Webb, 1993). It transmits two acoustic signals of 15 kHz and 18 kHz that interact within the water column to generate a secondary signal of lower frequency (1·5–4 kHz)

in the form of a narrow beam. This produces a vertical resolution of <30–40 cm within the upper 50–80 m of the sediment column at any water depth. The absolute position of any TOPAS reflection is accurate to within 10 cm (Webb, 1993).

A single giant piston core (core D13071) was recovered from the Selvage sediment-wave field during RRS *Discovery* cruise 225 in February 1997 (Fig. 1). This 13-m core has been logged with the multisensor core logger developed at Southampton Oceanography Centre (Best & Gunn, 1999), which records the P-wave velocity (ms^{-1}), wet bulk density using gamma ray attenuation (gcc^{-1}) and magnetic susceptibility (SI) of the core sediments. Core D13071 has also been logged visually and all sand-sized sediments sampled for mineralogical analysis.

A microfossil stratigraphy has been established for core D13071 based on coccolith ratios. The distribution of coccoliths has previously been tied to the oxygen isotope stratigraphy (e.g. Weaver, 1983) and provides a rapid, inexpensive and reliable method of dating the sedimentary sequence (Weaver & Kuijpers, 1983; Weaver, 1994). The technique is based on ratios of coccolith species, and zones are defined by appearance, extinction and cross-over points of dominant species. Within any zone, linear extrapolation through pelagic units is used to determine the age of a sedimentary horizon. Zones are only a few tens of thousands of years long, so potential errors are relatively small. This technique has enabled the sedimentation and wave migration rates in the Selvage wave field to be calculated.

THE SELVAGE SEDIMENT-WAVE FIELD

Wave distribution and morphology

The Selvage sediment-wave field lies at a water depth of 4285–4350 m on the continental rise north of the Selvage Islands (Figs 1 and 2). Upslope of the wave field is a break-of-slope at 4045 m, where a steep rock outcrop passes downslope into stratified sediments (Fig. 2). The gradient changes from 1·8° to 0·3° at this boundary. Between the break-of-slope and the top of the Selvage wave field is a zone of parallel- and wavy-stratified sediments that are interrupted by two transparent debris-flow deposits (Fig. 3). Small (<2 m high), irregular, non-migrating sediment waves occur in this zone. The well-developed sediment waves in the Selvage wave field occur immediately downslope from the lower debris-flow deposit and extend northwards for more than 20 km before dying out on the edge of the intraslope Agadir Basin (Fig. 4). Slope angles are between 0·22° and 0·21° (±0·05°) up to 20 km downslope from the top of the wave field, decreasing to 0·16–0·13° (±0·05°) beyond 20 km, where the sediment waves gradually merge into flat sea floor (Fig. 2). Wave heights (WH) reach a maximum of 6·2 m, and wavelengths (WL) vary from 0·4 km to 1·0 km (average 0·7 km). Wave

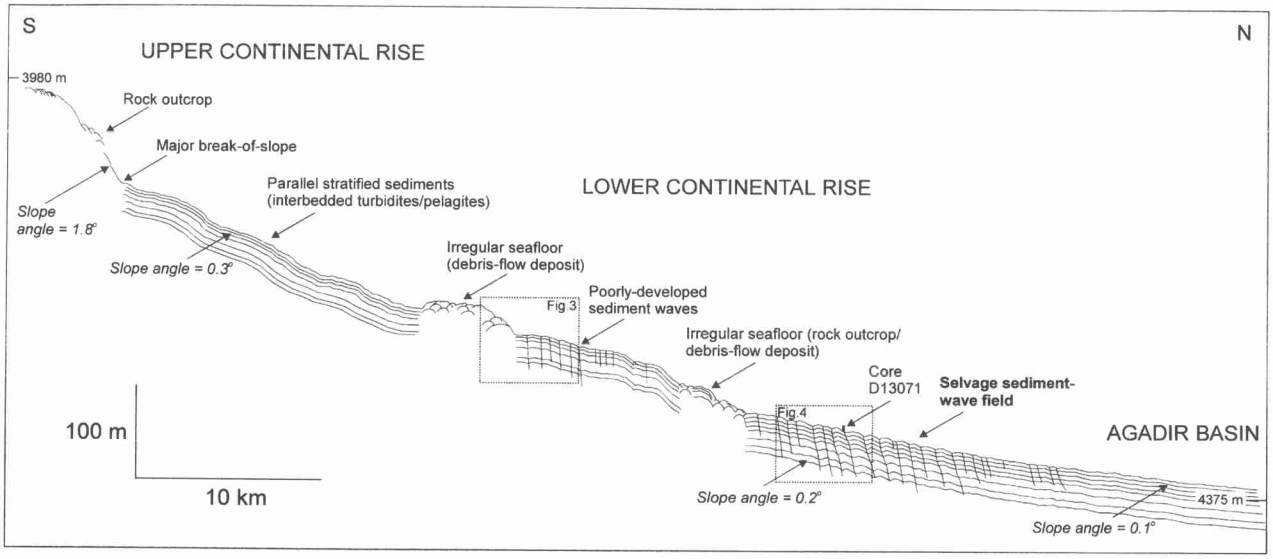

Fig. 2. Interpretative line drawing of TOPAS profile taken across the continental rise north of the Selvage Islands. Note the position of the Selvage sediment-wave field immediately downslope of the lower zone of irregular sea floor. The location of the TOPAS line is shown in Fig. 1. Dashed boxes indicate the locations of Figs 3 and 4.

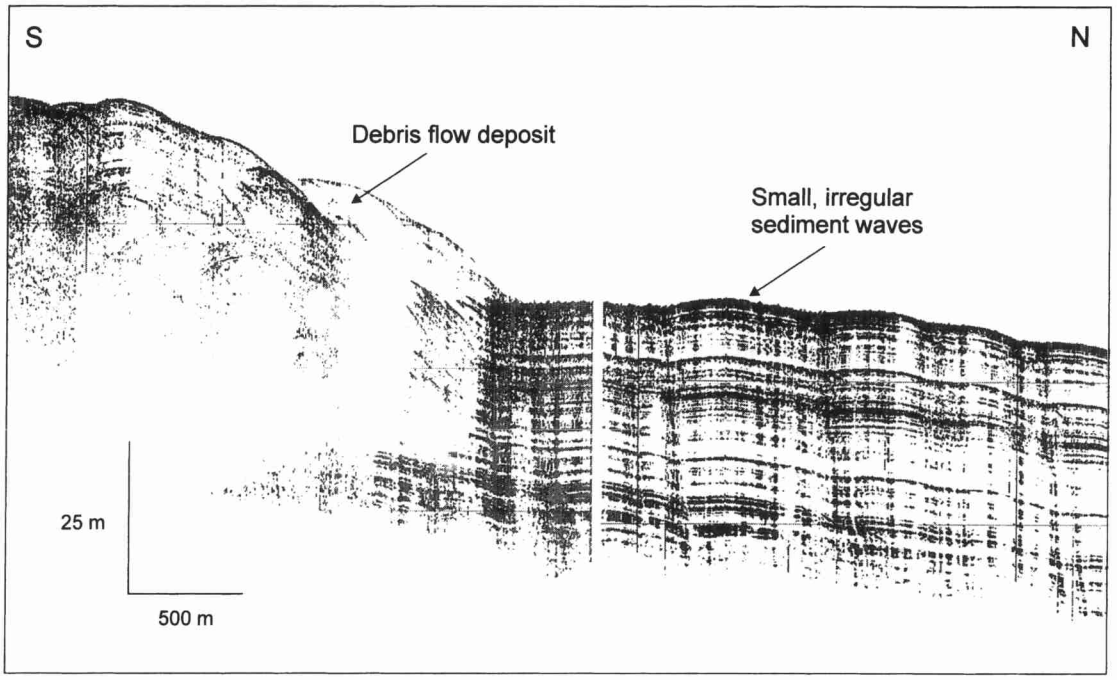

Fig. 3. TOPAS profile showing poorly developed sediment waves downslope of a transparent debris-flow deposit. The location of the profile is shown in Fig. 2.

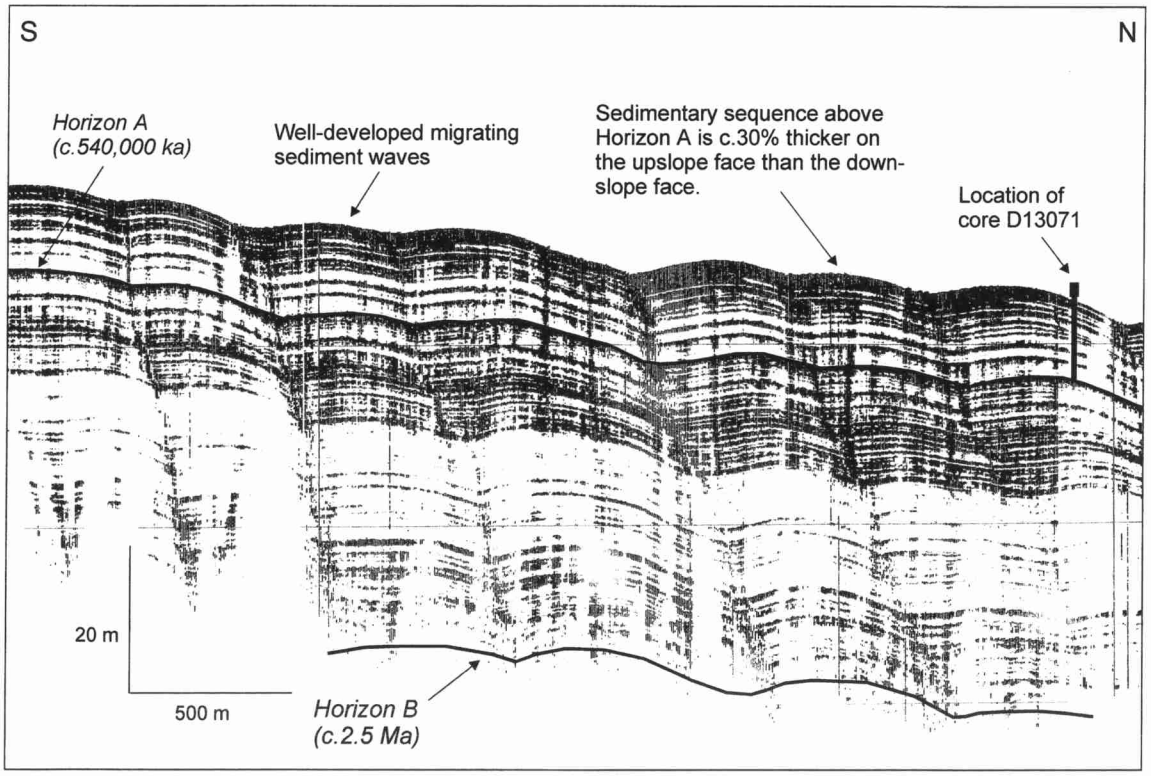

Fig. 4. TOPAS profile showing well-developed sediment waves in the Selvage sediment-wave field. Note the clear upslope migration of the waves. Position of core D13071 is indicated. The location of profile is shown in Fig. 2.

dimensions vary with distance downslope from the top of the wave field (Fig. 5). Sediment waves in the upper 10 km of the wave field show an overall increase in size downslope, and the largest sediment waves generally occur between 10 km and 15 km downslope from the top of the

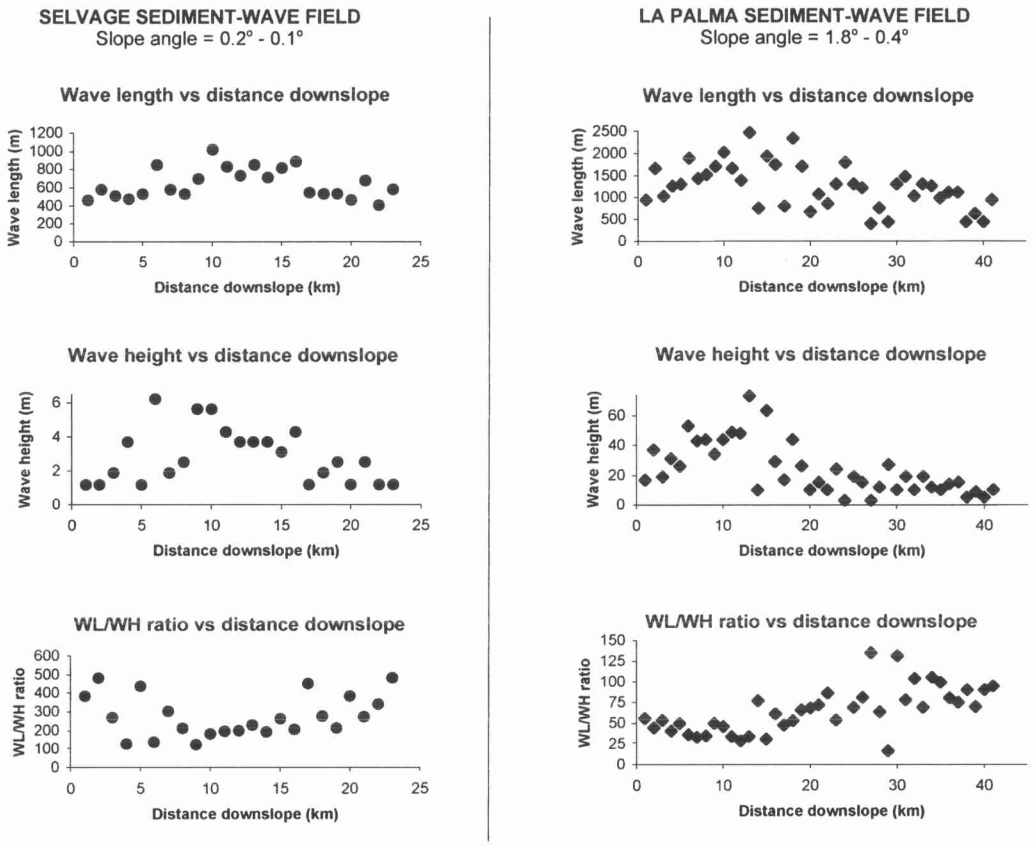

Fig. 5. Graphs showing variations in wave height (WH), wavelength (WL) and WL/WH ratio in the Selvage and La Palma sediment-wave fields (data for La Palma from Wynn *et al.* 2000a). Note how WH + WL peak about 10 km downslope in both wave fields and then gradually decrease downslope. The relatively small size of the Selvage sediment waves, compared with those off La Palma, results from the shallower slope angle and, consequently, lower TC flow velocity in the Selvage area.

wave field. Beyond 15 km downslope, the sediment waves show a progressive downslope decrease in size. WL/WH ratios show a similar pattern, with lowest values of 100–150 all occurring in the upper 10 km of the wave field. Between 10 km and 25 km downslope, the waves show progressively higher values (Fig. 5). The sediment waves are migrating upslope, and the sedimentary sequence on the upslope faces of the sediment waves, above horizon A, is about 30% thicker (±5%) than that on the downslope faces (Fig. 4).

Wave sediments

Core D13071 is 13 m long and was recovered from the downslope face of a sediment wave at a water depth of 4311 m (Figs 1 and 4). The core contains a sequence of interbedded turbidites and pelagic/hemipelagic marls and oozes (Fig. 6). Turbidites in this core are recognized using the following criteria: (1) a sharp or erosive base; (2) coarse sand/silt basal laminae; (3) normal size grading; and (4) reduced (or absent) bioturbation towards the base (Stow *et al.*, 1996; Fig. 7). Pelagic/hemipelagic sediments are dominated by white, foraminifera-rich, calcareous oozes and brown marls and clays. There are no indications of primary sedimentary structures within the pelagic/hemipelagic sediments (e.g. discontinuous laminae, lenses, sharp erosive contacts, abrupt lithological changes, etc.), suggesting an absence of significant bottom-current activity during deposition of the sequence (Stow *et al.*, 1996; Stow & Tabrez, 1998). Some of the fine-grained mud turbidites are bioturbated throughout, but are still distinguishable from fine-grained contourites and pelagic/hemipelagic sediments by gradation downwards into thin silty laminae at their base and/or sharp basal contacts with abrupt changes in sediment composition (Stow & Lovell, 1979; Stow & Tabrez, 1998; Fig. 7).

Four turbidites have sandy bases that have been sampled for mineralogical analysis. Generally,

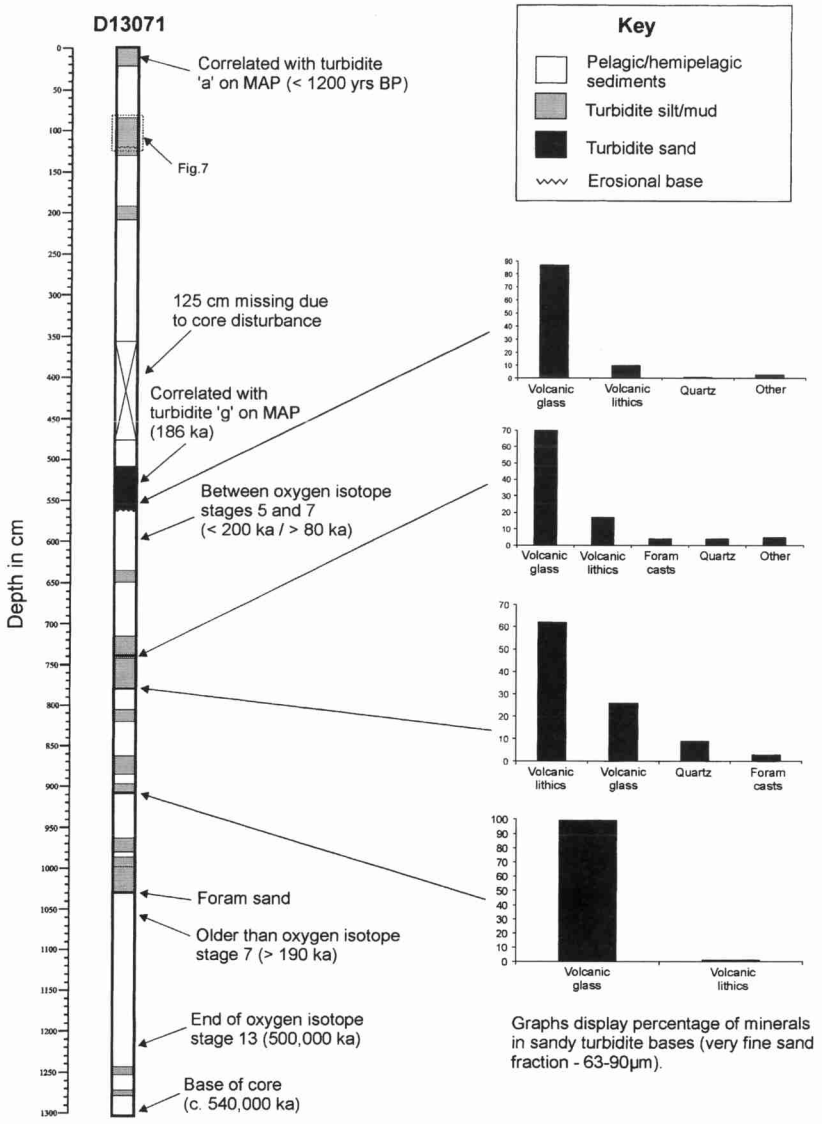

Fig. 6. Description of core D13071 recovered from the Selvage sediment-wave field, with graphs displaying the composition of sandy turbidite bases. MAP, Madeira Abyssal Plain. The location of the close-up interval in Fig. 7 is shown. Core location is shown in Figs 1 and 2.

the mineralogical assemblages of these turbidites are dominated by volcanic glass and volcanic lithic fragments, with minor amounts of quartz and biotite (Fig. 6). Volcanic minerals in turbidite bases commonly show a distinctive magnetic susceptibility 'spike' (Fig. 7). Biogenic constituents of turbidite sands include pelagic foraminifera (commonly present as siliceous casts), siliceous sponge spicules and fish teeth.

Dating of the pelagic intervals in core D13071, based on coccolith ratios, gives a date of ≈540 (±10) ka for the base of the core. This is based on linear extrapolation from a data point at 1175 cm, which represents the extinction of *Pseudoemiliania lacunosa* at 450 ka (Weaver, 1994). The overall sedimentation rate for the last 540 000 years is estimated at 2·4 (±0·3) cm 1000 years^{-1}. However, if turbidites are excluded, because turbidite deposition is instantaneous, the pelagic accumulation rate is only 1·7 (±0·3) cm 1000 years^{-1}. Using this dating control, it is possible to calculate the rate of upslope migration of the waves. In the last 540 000 years, the waves have migrated about 150 m upslope, giving a wave migration rate of 0·28 (±0·01) m 1000 years^{-1}. In addition, it is also possible to estimate the minimum age of the wave field. On TOPAS profiles, the wave morphology is visible to a subsurface depth of at least 60 m (Fig. 4). If it is assumed that the overall accumulation rate of 2·4 cm 1000 years^{-1} has remained relatively constant in the past, then it is possible to estimate the minimum age of the sediment waves. Evidence for a constant pelagic accumulation rate in the Canary Basin is revealed by ODP drilling results from the Madeira Abyssal Plain (Weaver *et al.*, 1998). On the plain, there

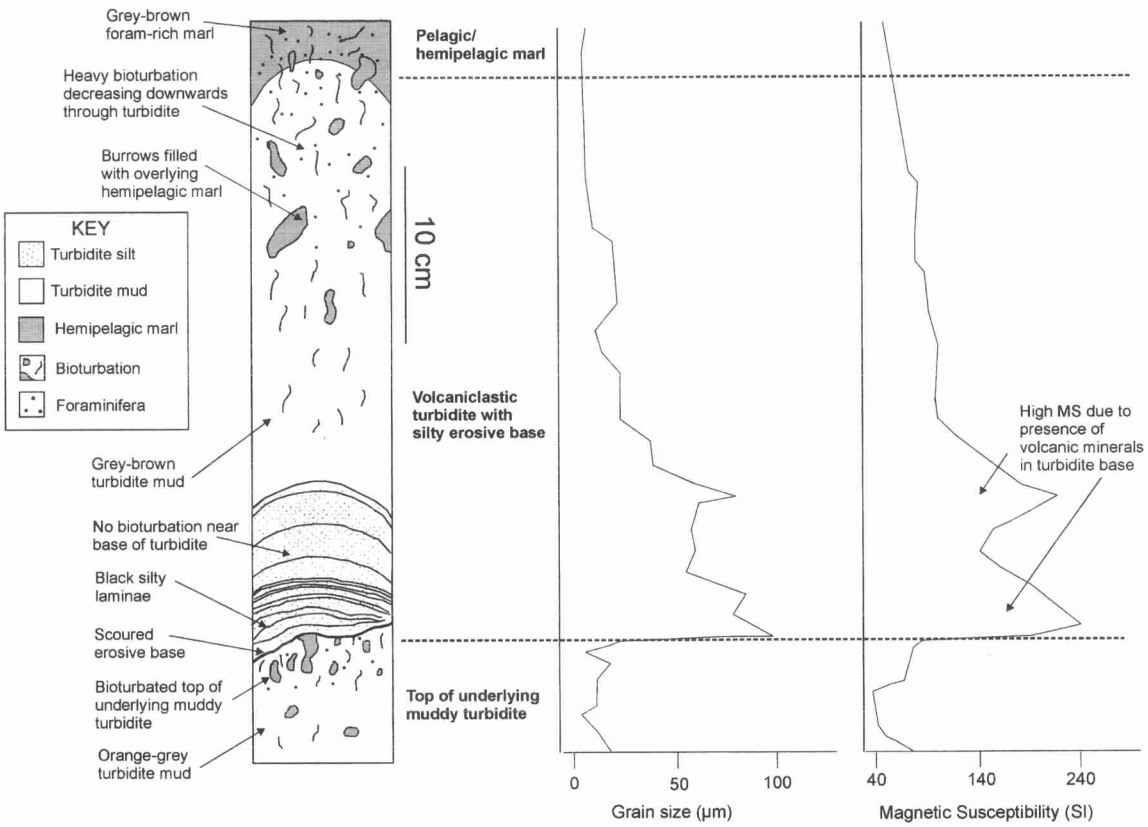

Fig. 7. Line drawing of part of the sedimentary sequence, including a volcaniclastic turbidite, in core D13071. The key diagnostic features used to identify turbidites in the core are shown, including (1) a scoured, erosive base; (2) dark, basal, volcanic silt laminae; (3) decreasing bioturbation downwards through turbidite; (4) fining-upwards sequence; (5) magnetic susceptibility spike at the base; and (6) sharp colour change at the base. The location of the interval shown is indicated in Fig. 6.

have been no major long-term changes in the depth of the CCD (>5400 m) in the last 3·5 Ma, which means that the pelagic accumulation rate should have remained relatively constant throughout the basin, including the area around the Selvage sediment-wave field. It is, however, not possible to calculate whether turbidite deposition, and hence the overall accumulation rate, has remained constant in the Selvage area. Despite this, it can be estimated that the sediment waves within the limits of TOPAS resolution have been forming for at least 2·5 million years.

DISCUSSION

Wave-generating processes

The sediment waves in the Selvage wave field are primary depositional bedforms and are clearly not gravity-driven compressional features (e.g. Hill *et al.*, 1982; Mulder & Cochonat, 1996), as they show evidence of upslope migration by asymmetric sediment deposition across the wave crests. The sediment waves have therefore been formed beneath either alongslope-flowing bottom currents or downslope-flowing turbidity currents. Although the Selvage sediment-wave field lies within a zone of north-east-flowing Antarctic Bottom Water (AABW), this bottom current is believed to be too weak at the present day to maintain the waves (Jacobi *et al.*, 1975; Embley, 1976; Lonsdale, 1982; Sarnthein *et al.*, 1982; Saunders, 1988). For example, a short-term, current-meter study undertaken in the vicinity of the Canary Islands recorded near-bed AABW flowing to the north-east at velocities of just 3–6 cm^{-1} (Lonsdale, 1982). Flood (1998) found that sediment waves formed beneath bottom currents at velocities of 9–50 cm s^{-1}. Although it is possible that AABW flow across the Selvage wave field was stronger in the past, there is no evidence of significant bottom-current sedimentation or reworking in core D13071. Detailed examination of pelagic/hemipelagic sediments in the core has

revealed no indication of the primary sedimentary structures (e.g. discontinuous laminae, lenses, sharp erosive contacts, abrupt lithological changes, etc.) that would be expected to occur under bottom currents with sufficient velocity to generate sediment waves. In addition, Jacobi *et al.* (1975) discovered that the wave crests are aligned parallel to the slope. This alignment is not compatible with existing models of bottom-current sediment waves on slopes, which predict that the wave crests will be oblique to the bottom-current flow and the regional bathymetric gradient (Blumsack & Weatherly, 1989; Blumsack, 1993).

A turbidity current origin for the Selvage wave field is favoured for the following reasons:

1 Core sediments. Core D13071 contains a total of 15 turbidites (Fig. 6) that are recognized by a sharp or erosive base, coarse sand/silt basal laminae, normal size grading and reduced (or absent) bioturbation towards the base (Fig. 7). The presence of several turbidites in core D13071 indicates regular TC flow across the wave field. In addition, there is no evidence of significant bottom-current sedimentation or reworking in the fine-grained sediments, and this strongly suggests a TC origin for the sediment waves.

2 Crest alignment. The alignment of wave crests parallel-to-slope is typical of TC sediment waves (Table 1). Sediment waves generated by bottom currents flowing parallel-to-slope generally show an oblique crest alignment (Blumsack & Weatherly, 1989; Blumsack, 1993).

3 Wave dimensions. The sediment waves show a progressive downslope decrease in wave height and wavelength in the lower section of the wave field (Fig. 5). This pattern is a response to decreasing slope gradient and flow velocity and is a common feature of TC sediment waves (Table 1). Sediment waves generated beneath bottom currents typically display more irregular dimensions (e.g. Cunningham & Barker, 1996; Howe *et al.*, 1998).

The Selvage sediment-wave field is therefore interpreted as having formed beneath unconfined turbidity currents, in a similar fashion to that described from the La Palma sediment-wave field in the western Canary Islands (Wynn *et al.*, 2000a). There is no evidence for the existence of turbidity current channels in the area of the Selvage wave field, so turbidity currents are believed to flow as unconfined sheet flows across the continental rise. This setting is very similar to that described for sediment waves on channel-lévee backslopes (e.g. Normark *et al.*, 1980; Carter *et al.*, 1990; Piper & Savoye, 1993; Lewis *et al.*, 1998; Nakajima *et al.*, 1998; Piper *et al.*, 1999). The upslope migration direction of the waves and the dominantly volcanic mineral assemblage indicates formation beneath turbidity currents originating from the flanks of volcanic islands to the south (Fig. 1). The Selvage Islands may be the source for some of the smaller flows, but are probably too stable and eroded to provide enough sediment to feed the larger flows. Good evidence of a Canary Island source for at least some of the flows is given in a recent study of turbidite deposition in the Agadir Basin (Wynn *et al.*, 2000b), which demonstrates that the turbidite in core D13071 between 520 and 570 cm (Fig. 6) can be correlated with turbidite 15 in the Agadir Basin and turbidite '*g*' on the Madeira Abyssal Plain. Turbidite '*g*' is dated at 186 ka and is sourced from the north flank of Tenerife (Rothwell *et al.*, 1992; Masson, 1994).

Wave migration

The migration rates of waves estimated for the Selvage sediment-wave field can be compared with those recorded in sediment-wave sequences elsewhere and appear to demonstrate a clear link between sedimentation rate, especially the frequency of turbidity currents, and wave migration rate. Carter *et al.* (1990) described a sediment-wave field on the backslope of the Bounty Channel levée that was formed beneath unconfined turbidity currents. The overall sedimentation rate was estimated at 13–26 cm 1000 years^{-1}, and the wave migration rate was between 2·8 and 5·6 m 1000 years^{-1}. Sediment waves generated beneath bottom currents on the Feni Ridge were found to have a sedimentation rate of 2·7–4·5 cm 1000 years^{-1} and a wave migration rate of 0·25 m 1000 years^{-1} (Lonsdale & Hollister, 1979). The Selvage sediment waves have a sedimentation rate of 2·4 cm 1000 years^{-1} and a wave migration rate of 0·28 m 1000 years^{-1}, and are therefore more comparable with the sediment waves generated beneath bottom currents on the Feni Ridge. This is because turbidity currents are relatively infrequent on the continental rise south of the Canary Islands (Wynn *et al.*, 2000b), leading to a low sedimentation rate and, consequently, a low wave migration rate.

It is important to note that, on TOPAS profiles (Fig. 4), the sediment waves appear to be migrating upslope at a regular rate. This seems unusual, as nearly three-quarters of the sediments in core

D13071 are pelagic and hemipelagic sediments, which would be expected to drape the wave morphology evenly through vertical settling. Wave migration should therefore only occur during deposition of turbidites, which make up just 28% of the core. A possible solution is that irregular wave migration will not be resolvable on TOPAS profiles, as any small-scale irregularities in the migration profile will probably be smoothed over, making upslope migration appear regular over time. Another possibility is that, although large-scale, instantaneous turbidity currents are undoubtedly the key process in controlling wave morphology and migration, other processes may also be involved. For example, fine-grained terrigenous sediment can be transported downslope by slow, dilute, 'continuous' turbidity currents (Damuth, 1977; Damuth *et al.*, 1988) and may contribute to wave formation and migration. In addition, although bottom currents are clearly not responsible for the generation of the Selvage sediment waves (as shown by the wave orientation and sedimentology), a weak bottom current may redistribute pelagic/hemipelagic sediments unevenly across the wave crest, also contributing to the overall upslope migration. Therefore, although large, infrequent turbidity currents are the dominant force shaping and maintaining the waves, the possibility that slow, dilute, continuous, turbidity/bottom currents are contributing to upslope wave migration cannot be ruled out.

Turbidity current flow characteristics

The flow characteristics for turbidity currents can be constrained by simple numerical modelling, and this is attempted for flows crossing the Selvage sediment-wave field. First, an attempt is made to calculate the internal Froude number, and this value is combined with wavelength to estimate flow thickness; flow velocity is calculated using two different methods, one based on grain size and the other on internal Froude number and sediment concentration.

Internal Froude number

The internal Froude number (*Fi*) for a turbidity current can be calculated using a combination of slope gradient (*sin* β), drag coefficient at the bed (C_f) and entrainment coefficient at the upper interface (E). Generally, *Fi* decreases with a reduction in slope gradient and is lower in less turbulent flows (Bowen *et al.*, 1984). At $Fi = 1$, also known as critical flow, the turbidity current is in a relatively steady state, and the head and body travel at a similar speed (Middleton, 1966). The following calculations of *Fi* are based on Eq. 1 from Bowen *et al.* (1984):

$$Fi^2 = \frac{\sin\beta}{C_f + E} \tag{1}$$

where Fi = internal Froude number, *sin* β = slope angle, C_f = drag coefficient and E = entrainment coefficient.

In the Selvage sediment-wave field, the slope angle varies from 0·22° to 0·13°. Suggested values for the drag coefficient (C_f) in channelized turbidity currents are in the range of $3–5 \times 10^{-3}$ (e.g. Komar, 1975; Bowen *et al.*, 1984). However, in the case of unconfined flows crossing the slope and rise, a lower figure may be more applicable. Therefore, a range of C_f values is used, varying from the minimum possible value of 5×10^{-4} for a smooth, artificial bed to a maximum of 5×10^{-3} for channelized flows crossing a gravel bed. The entrainment coefficient (E) for most turbidity currents varies between 5×10^{-4} and 6×10^{-3} (Bowen *et al.*, 1984). Using Eq. 1, these figures give a range of Froude numbers from $Fi = 1·9–0·6$ on the maximum slope of 0·22° in the upper wave field to $Fi = 1·5–0·5$ on the minimum slope of 0·13° in the lower wave field. Taking the mean values, *Fi* decreases from 1·25 to 1 downslope. These figures are in agreement with previous research on unconfined turbidity currents (e.g. Normark *et al.*, 1980) and suggest that the turbidity currents may have passed from supercritical to subcritical flow on their passage across the wave field.

Flow thickness

Equation 2 illustrates the relationship between sediment wavelength (L), flow thickness (h) and internal Froude number (*Fi*) and has been modified from Normark *et al.* (1980):

$$h = \frac{L}{2\pi Fi^2} \tag{2}$$

where h = flow thickness and L = wavelength.

In the Selvage sediment-wave field, L reaches a maximum of 1 km about 10 km downslope from the top of the wave field, before showing a gradual decrease to a minimum of 0·4 km about 25 km downslope. Using Eq. 2 and accounting for variations in *Fi* as demonstrated by Eq. 1, it can be shown that, from 0 km to 10 km downslope, flow thickness increases from 20–200 m to

45–450 m. Flow thickness then gradually decreases downslope to a minimum of 30–260 m at 25 km downslope. These values are comparable with those estimated in previous studies (e.g. Normark *et al.*, 1980; Wynn *et al.*, 2000a). Between 10 km and 25 km, flow thickness decreases downslope by about 60% over a total distance of 15 km. This compares with a downslope decrease in flow thickness of 83% over 25 km for turbidity currents crossing the La Palma sediment-wave field (Wynn *et al.*, 2000a) and 86% over 15 km for turbidity currents crossing the Monterey Fan levée backslope (Normark *et al.*, 1980). This relatively rapid reduction in flow thickness is expected for unconfined, spreading flows on open slopes (Komar, 1975). It should be noted that the wide range of flow thicknesses obtained using Eq. 2 highlights the sensitivity of this equation to relatively minor changes in *Fi* and leads to variations in flow thickness of an order of magnitude.

Flow velocity based on maximum settling velocity

An indication of flow velocity can be obtained by estimating the maximum settling velocity (w), which is a function of the turbidite grain size. Generally, turbidites in core D13071 contain thin sandy bases with a maximum grain size of about 200 μm (2·3 ϕ). Above these bases, silt laminae of modal grain size 30–60 μm (4–5 ϕ) are often developed, and the top of the turbidite is composed of fine silts and muds (<30 μm or 5 ϕ). Assuming that these relatively fine-grained sediments are carried in the flow as suspended load, then $b = 1{\cdot}25$ in the following equation (Bowen *et al.*, 1984):

$$u = \frac{bw}{\sqrt{C_f}} \tag{3}$$

where u = flow velocity, b = a parameter linking settling velocity to frictional velocity, w = settling velocity of the suspended sediment and C_f = drag coefficient.

A range of predicted flow velocities are obtained if variations in C_f are accounted for, as discussed above. For the sandy turbidite bases, the maximum flow velocity attainable at the time of deposition is between 42 and 125 cm^{-1}. For deposition of the overlying silty laminae, velocities range from 6 to 38 cm^{-1}. Finally, the fine-grained turbidite tops are deposited at velocities of <6–38 cm^{-1}. These figures are very similar to those obtained by Stow & Bowen (1980), Normark *et al.* (1980) and Bowen *et al.* (1984) for turbidity currents on submarine fans.

Flow velocity based on internal Froude number and sediment concentration

Estimates of flow velocity can also be obtained using the following equation (Piper & Savoye, 1993):

$$u^2 = \Delta p C g h Fi^2 \tag{4}$$

where Δp = (grain density–TC density)/sea-water density, C = volume concentration and g = gravitational acceleration.

C is a dimensionless number that represents the sediment concentration. For fine-grained, unconfined turbidity currents, previous research has shown that C is in the range 10^{-5}–10^{-6} (Normark *et al.*, 1980). However, it should be noted that Eq. 4 is sensitive to changes in C, which is one of the most poorly constrained variables in TC modelling. Existing data indicate that C can vary by several orders of magnitude depending on the type of flow involved (e.g. Normark *et al.*, 1980; Bowen *et al.*, 1984; Piper & Savoye, 1993). Flow thickness (h) has been shown to vary between 20 and 450 m, and Fi^2 ranges from 3·61 to 0·25. When these variables are entered into Eq. 4, it can be shown that velocities in the upper wave field range from 3 to 130 cm^{-1}, and in the lower wave field range from 2 to 80 cm^{-1}. The maximum value of 130 cm^{-1} is very similar to that of 125 cm^{-1} obtained from grain size data using Eq. 3. These maximum values probably represent the velocity at the head of the turbidity current, as this is where sediment concentration and flow thickness are highest. The lower values probably represent the slower moving tail of the turbidity current, where sediment concentration and flow thickness are much reduced.

New insights into the formation of deep-water sediment waves

Having established that the Selvage sediment-wave field has formed beneath unconfined turbidity currents, the discussion will now focus on the two existing models for sediment-wave formation and investigate which model is most applicable to the Selvage sediment waves. The applicability of each model to the formation of both bottom-current and TC sediment waves is discussed in turn.

The lee-wave model and bottom-current sediment waves

The link between internal lee waves and sediment-wave formation was reviewed by Allen (1984) with respect to sediment waves generated beneath bottom currents. The lee-wave model was further developed by Flood (1988), but was only applicable to situations in which wave crests were oriented perpendicular to the flow. Blumsack & Weatherly (1989) and Blumsack (1993) adapted the model to account for sediment waves on slopes with crests aligned oblique to bottom-current flow direction. The lee-wave model is dependent upon a weakly stratified water column and an initial sea-floor perturbation to initiate the development of lee-waves within a bottom-current flow. The model predicts that the formation of bottom-current sediment waves will generally only occur at current velocities of 9–50 cm^{-1} (Flood, 1988). At these velocities, internal lee-waves are generated within the bottom current, leading to increased flow velocities on the downstream face of a sediment wave. This causes reduced deposition, non-deposition or erosion on the downstream flank. As the current slows on the upstream face of the wave, deposition occurs, leading to an overall upcurrent wave migration. When tested against observations in the Argentine Basin, the lee-wave model appeared to show good agreement with real data sets (Flood, 1988; Blumsack & Weatherly, 1989). However, this model is not applicable to the Selvage sediment-wave field because, as discussed previously, the crest orientation is parallel to the slope and the bottom-current flow (Jacobi *et al.*, 1975). This crest alignment is not compatible with the lee-wave model proposed by Flood (1988), which is only applicable to sediment waves with crests aligned perpendicular to the flow direction. It is also incompatible with the advanced lee-wave model of Blumsack & Weatherly (1989) and Blumsack (1993), which predicts that most sediment waves on slopes will develop crest orientations that are oblique to the flow direction.

The lee-wave model and TC sediment waves

The lee-wave model of Flood (1988) has also been applied to TC sediment waves (Lewis, 1994; Howe, 1996). This application seems logical, given that the morphology and internal architecture of sediment waves generated beneath bottom and turbidity currents are very similar, suggesting a common process of formation. In addition, the present study has revealed that the relationship between sedimentation rate and wave migration rate in the Selvage sediment-wave field is very similar to that described for a field of bottom-current sediment waves on the Feni Ridge (Lonsdale & Hollister, 1979). As lee-waves are generated when a density-stratified current flows over an irregular sea floor (Flood, 1988), it is possible that, under certain conditions, turbidity currents flowing over uneven topography will achieve sufficient internal density stratification to allow lee-wave formation (e.g. Stacey & Bowen, 1988; Normark & Piper, 1991; Kneller & Branney, 1995). The condition for lee wave formation in a stratified flow depends on the parameter U/NH, where U is the velocity, N is the buoyancy frequency, and H is the flow thickness (Turner, 1973). This parameter, which may be called the 'stratification' Froude number F_s, differs from F_i, the internal Froude number of Eq. 1, which is in effect an 'overall' Froude number (Turner, 1973). For lee waves to form, F_s must be $<1/\pi$, i.e. less than ≈ 0.318 (Turner, 1973). In the case of the turbidity currents associated with the Selvage sediment-wave field, no data are available to estimate F_s directly. However, measurements of suspended-sediment profiles in rivers (Schrimpf, 1986) and in experimental turbidity currents (Parker *et al.*, 1987) indicate that F_s is unlikely to fall below a value of $\approx 0.8\ F_i$. For turbidity currents associated with the Selvage sediment-wave field, F_i is calculated to be 0.5–1.9, which would give minimum F_s values of 0.4–1.5, too great for the generation of lee waves.

Among the seven other TC sediment-wave fields considered (Table 1), calculated F_i values range from 0.4 to 2.4, which would give minimum F_s values of 0.32–1.9, again just failing to meet the criterion $F_s < 1/\pi$. These results suggest that lee waves cannot be generated within the types of turbidity currents responsible for creating and maintaining the Selvage and other TC sediment-wave fields.

The antidune model and bottom-current sediment waves

Several studies have discussed the possible application of the antidune model to sediment waves generated beneath bottom currents (Hand, 1974; Kolla *et al.*, 1980; McCave & Tucholke, 1986). However, evidence presented by Allen (1984) indicates that this is impossible because, for most bottom currents, $Fi < 0{\cdot}3$ (based on observed flow

thickness, density and density differences). This is well below the lower limit of $Fi = 0{\cdot}844$ required for antidune formation and shows that antidune conditions cannot be generated within most bottom currents. Unfortunately, there is no information available on flow thickness or concentration for bottom currents flowing over the Selvage sediment waves, and it is therefore not possible to estimate *Fi* for these flows. However, as most bottom currents generally display similar characteristics (Allen, 1984), it is unlikely that the bottom currents crossing the Selvage sediment waves will have Froude numbers within the antidune existence limits.

The antidune model and TC sediment waves

There is better agreement in the literature that TC sediment waves can form as antidunes. Hand *et al.* (1972) first noted that large-scale antidunes (with wavelengths in the order of tens to hundreds of metres) could occur as a result of the formation of surface waves at the interface between a turbidity current and seawater. Normark *et al.* (1980) then developed a two-layer antidune model for sediment waves formed beneath unconfined turbidity currents on channel levées. This model accounts for the condition in which a dense turbid underflow moves beneath stationary seawater and reveals several features that are compatible with actual observations. For example, the calculated values of sediment concentration and flow thickness, derived from the antidune model, are very similar to those taken from first-hand observations in similar settings (e.g. Stow & Bowen, 1980; Piper & Savoye, 1993). In addition, Normark *et al.* (1980) stated that 'the depth of flow is approximately one-sixth of the wavelength', implying that, as flow thickness decreases, wavelength also decreases (see Eq. 2). This appears to be the case in reality, whereby the majority of TC sediment waves display an overall decrease in wavelength downslope (Table 1), and is compatible with the observations of Komar (1975), who argued that levée overbank (unconfined) flows will become thinner downslope as they expand laterally. Observed and calculated occurrences of antidunes suggest that they form beneath flows in which $Fi = 0{\cdot}844$–$1{\cdot}77$ (Allen, 1984). For turbidity currents crossing the Selvage sediment-wave field, $Fi = 0{\cdot}5$–$1{\cdot}9$, which is in good agreement with the antidune existence limits. The minimum value of $Fi = 0{\cdot}5$ is just below the lower limit of antidune formation (Allen, 1984) and may explain why the Selvage sediment waves die out downslope on slope angles <0·1°. A number of other TC sediment-wave fields (Table 1) are crossed by turbidity currents with $Fi \approx 0{\cdot}4$–$2{\cdot}4$ and are therefore also close to the antidune existence limits.

The pattern of wave dimensions in the Selvage sediment-wave field may give some indication of how turbidity currents interacting with sea-floor topography can inhibit sediment-wave development. The largest sediment waves occur about 10 km downslope from the top of the wave field (Fig. 5) and then show a progressive downslope decrease in dimensions. However, in the upper 10 km of the wave field, the sediment waves show an overall downslope increase in dimensions, which is unexpected as the slope angle in this area remains fairly constant at 0·2°. A possible explanation may be linked to the fact that sediment waves in the upper 10 km of the wave field occur immediately downslope of a buried rock outcrop/debris flow deposit (Fig. 2). Turbidity currents will have flowed over or around this obstacle, although as its lateral extent is unknown, this cannot be qualified with certainty. However, Alexander & Morris (1994) found that, for experimental unconfined flows, where obstacle height is significantly smaller than flow thickness, the flow will continue over the obstacle without being deflected. As the height of the topographic obstacle upslope of the Selvage wave field is only about 20% of the flow thickness, it seems likely that the flow will pass over the obstacle in this instance. Alexander & Morris (1994) also suggested that flow over even relatively small obstacles can influence bedform character and distribution. Flows travelling over the top of the deposit may have undergone a hydraulic jump on leaving the obstacle, as there is a distinct break-of-slope at its downslope boundary. The slope angle changes from 0·6° to 0·2° at this boundary, leading to a change in *Fi* of 1·0–3·2 to 0·6–1·9 (based on Eq. 1). This may therefore correspond to a change from super- to subcritical conditions and the development of a hydraulic jump. During a hydraulic jump, turbidity currents increase in thickness and generate intense turbulence (Komar, 1971). Speculatively, this increase in turbulent energy could prevent the development of the optimum conditions necessary for antidune formation. Allen (1984) stated that near-stationary bed and surface waves are necessary for the development of antidunes and that, in turbidity currents, the surface waves are probably developed on interfaces within the flow. Therefore, if these interfaces are disrupted by the

increased turbulence of a hydraulic jump, antidune development may be affected. In addition, experimental work by Garcia & Parker (1989) revealed that the maximum deposition of sediment carried as suspended load occurred downstream of the jump. This may also explain why the largest waves are 10 km downslope of the topographic obstacle, as this is probably where the zone of maximum sediment deposition occurs.

A similar pattern of wave dimensions is observed in the La Palma sediment-wave field (Fig. 5), with the largest waves occurring between 10 km and 20 km downslope from an area of steep rock outcrop/slump deposits (Wynn *et al.*, 2000a). This pattern is probably also related to the factors discussed above. However, in both examples, the 10–20 km 'lag' between the edge of the obstacle and the maximum wave dimensions has yet to be satisfactorily explained, and further data need to be collected on the exact nature and orientation of these topographic obstacles before this interpretation can be developed further.

Wider implications of this study

The interpretation that the Selvage sediment-wave field is formed beneath unconfined turbidity currents has important implications for studies of other sediment-wave fields in the deep ocean. The Selvage sediment waves occur in a linear belt that runs along the lower continental rise parallel to the bathymetric gradient in a setting that was previously seen as being typical of bottom current-dominated settings (e.g. Embley & Langseth, 1977). However, this study has revealed that, in areas where the lower rise is crossed by unconfined sheet flows, a linear band of TC sediment waves can occur. A similar situation occurs on channel-levée backslopes, where sediment waves generated by unconfined sheet flows are generally confined to a narrow band oriented parallel to the bathymetric gradient (e.g. Normark *et al.*, 1980; Carter *et al.*, 1990; Nakajima *et al.*, 1998). It is therefore important to recognize that sediment waves generated by turbidity currents are not just confined to channels and their levées, but may also occur in other deep-water settings with turbidity current input.

CONCLUSIONS

Sediment waves in the Selvage wave field display characteristics similar to those described from channel-levée backslopes and are interpreted as having formed beneath unconfined turbidity currents. Sedimentological analysis of sandy turbidite bases indicates that the flows were probably sourced from the flanks of the volcanic Canary Islands to the south. The wave migration rate in the Selvage wave field is similar to that estimated for bottom-current sediment waves on the Feni Ridge, but is considerably lower than the wave migration rate on the Bounty Channel levées. This is compatible with the relatively low sedimentation rate and TC frequency in the vicinity of the Selvage sediment-wave field.

Application of existing models for sediment-wave formation indicates that the antidune model is most applicable to sediment waves formed beneath unconfined turbidity currents, including the Selvage sediment waves. Slope angles across the Selvage sediment-wave field are very close to the lower limit for antidune formation (based on the relationship between Froude number and slope angle), and this may explain the relatively small size of the waves and their disappearance downslope as the slope angle decreases. Estimates of flow thickness based on wavelength and Froude number suggest that turbidity currents initially increase in thickness downslope of an obstacle and reach a maximum flow thickness of 45–450 m about 10 km from the top of the wave field. Between 10 km and 25 km downslope, there is a gradual decrease in flow thickness to a minimum of 30–260 m.

Several key questions regarding TC flow processes need to be answered before models of sediment-wave formation can be developed further. For example, is the relationship between Froude number and slope angle accurate and is it applicable to unconfined turbidity currents? Can the antidune model be applied to coarse-grained sediment waves in channels? How is sediment wave formation affected by flow over obstacles? Unfortunately, because of the nature, environment and unpredictability of natural turbidity currents, field observation of flow processes is generally impossible. However, carefully constructed laboratory experiments could lead to an increased understanding of the controls on sediment-wave formation and may help in the prediction of their occurrence in subsurface turbidite systems.

ACKNOWLEDGEMENTS

The authors would like to acknowledge the expertise and enthusiasm of the Masters, officers

and crew present on RRS *Discovery* cruise 225 and RV *Hesperides* cruise MAYC-95. The RV *Hesperides* cruise was carried out within the framework of project AMB-95-0196. R.B.W. acknowledges the provision of PhD funding from the University of Southampton and the Southampton Oceanography Centre Challenger Division. B. Alonso and J. Baraza are thanked for their contribution to the collection and interpretation of the TOPAS profiles. Dave Gunn provided technical assistance with core logging. Special thanks go to Henry Pantin for his assistance in comparing different types of Froude number when assessing the validity of the lee-wave model. This paper benefited greatly from the constructive reviews provided by John Damuth and Stephen Morris and the thorough editing of Jim Best.

NOTATION

b	parameter linking settling velocity to frictional velocity
C	volume concentration
C_f	drag coefficient
Fi	internal Froude number
F_s	stratification Froude number
E	entrainment coefficient
g	gravitational acceleration (m s^{-2})
h	flow thickness (m)
L	wavelength (m) (in equations)
N	buoyancy frequency
$\sin \beta$	slope angle
u	flow velocity (m s^{-1})
w	settling velocity of the suspended sediment (m s^{-1})
WH	wave height (m)
WL	wavelength (km)
Δp	(grain density–TC density)/sea-water density (kg m^{-3})
ϕ	phi (grain size units)

REFERENCES

Alexander, J. and **Morris, S.** (1994) Observations on experimental, non-channelized, high-concentration turbidity currents and variations in deposits around obstacles. *J. Sed. Res.*, **A64,** 899–909.

Allen, J.R.L. (1984) *Sedimentary Structures, Their Character and Physical Basis.* Elsevier, Amsterdam, 663 pp.

Best, A.I. and **Gunn, D.E.** (1999) Calibration of marine sediment core loggers for quantitative acoustic impedance studies. *Mar. Geol.*, **160,** 137–146.

Blumsack, S.L. (1993) A model for the growth of mudwaves in the presence of time-varying currents. *Deep-Sea Res. II,* **40,** 963–974.

Blumsack, S.L. and **Weatherly, G.L.** (1989) Observations of the nearby flow and a model for the growth of mudwaves. *Deep-Sea Res.*, **36,** 1327–1339.

Bowen, A.J., Normark, W.R. and **Piper, D.J.W.** (1984) Modelling of turbidity currents on Navy submarine fan, California Continental Borderland. *Sedimentology*, **31,** 169–185.

Carter, L., Carter, R.M., Nelson, C.S., Fulthorpe, C.S. and **Neil, H.L.** (1990) Evolution of Pliocene to Recent abyssal sediment waves on Bounty Channel levees, New Zealand. *Mar. Geol.*, **95,** 97–109.

Cunningham, A.P. and **Barker, P.F.** (1996) Evidence for westward-flowing Weddell Sea Deep Water in the Falkland Trough, western South Atlantic. *Deep-Sea Res.*, **45,** 643–654.

Damuth, J.E. (1977) Late Quaternary sedimentation in the western equatorial Atlantic. *Geol. Soc. Am. Bull.*, **88,** 695–710.

Damuth, J.E. (1979) Migrating sediment waves created by turbidity currents in the northern South China Basin. *Geology*, **7,** 520–523.

Damuth, J.E., Flood, R.D., Kowsmann, R.O., Belderson, R.H. and **Gorini, M.A.** (1988) Anatomy and growth pattern of Amazon deep-sea fan as revealed by long-range side-scan sonar (GLORIA) and high-resolution seismic studies. *AAPG Bull.*, **72,** 885–911.

Droz, L., Rigaut, F., Cochonat, P. and **Tofani, R.** (1996) Morphology and recent evolution of the Zaire turbidite system (Gulf of Guinea). *Geol. Soc. Am. Bull.*, **108,** 253–269.

Embley, R.W. (1976) New evidence for occurrence of debris flow deposits in the deep sea. *Geology*, **4,** 371–374.

Embley, R.W. and **Langseth, M.G.** (1977) Sedimentation processes on the continental rise of northeastern South America. *Mar. Geol.*, **25,** 279–297.

Ewing, M., Aitken, T. and **Eittreim, S.** (1968) Giant ripples in the Madagascar Basin. *Trans. Am. Geophys. Union*, **49,** 218–232.

Flood, R.D. (1988) A lee wave model for deep-sea mudwave activity. *Deep-Sea Res.*, **35,** 973–983.

Fox, P.J., Heezen, B.C. and **Harian, A.M.** (1968) Abyssal antidunes. *Nature*, **220,** 470–472.

Garcia, M.H. and **Parker, G.** (1989) Experiments on hydraulic jumps in turbidity currents near a canyon-fan transition. *Science*, **245,** 393–396.

Hand, B.M. (1974) Supercritical flow in density currents. *J. Sed. Petrol.*, **44,** 637–648.

Hand, B.M., Middleton, G.V. and **Skipper, K.** (1972) Antidune cross-stratification in a turbidite sequence, Cloridorme Formation, Gaspe, Quebec. *Sedimentology*, **18,** 135–138.

Hill, P.R., Moran, K.M. and **Blasco, S.M.** (1982) Creep deformation of slope sediments in the Canadian Beaufort Sea. *Geo-Mar. Lett.*, **2,** 163–170.

Howe, J.A. (1996) Turbidite and contourite sediment waves in the northern Rockall Trough, North Atlantic Ocean. *Sedimentology*, **43,** 219–234.

Howe, J.A., Livermore, R.A. and **Maldonado, A.** (1998) Mudwave activity and current-controlled sedimentation in Powell Basin, northern Weddell Sea, Antarctica. *Mar. Geol.*, **149,** 229–241.

Jacobi, R.D., Rabinowitz, P.D. and **Embley, R.W.** (1975) Sediment waves on the Moroccan continental rise. *Mar. Geol.*, **19,** 61–67.

Johnson, G.L. and **Schneider, E.D.** (1969) Depositional ridges in the North Atlantic. *Earth Planet. Sci. Lett.*, **6,** 416–422.

Kenyon, N.H. and **Belderson, R.H.** (1973) Bedforms of the Mediterranean undercurrent observed with side-scan sonar. *Sed. Geol.*, **9,** 77–99.

Kenyon, N.H., Millington, J., Droz, L. and **Ivanov, M.K.** (1995) Scour holes in a channel-lobe transition zone on the Rhone Cone. In: *Atlas of Deep Water Environments: Architectural Style in Turbidite Systems* (Eds K.T. Pickering, R.N. Hiscott, N.H. Kenyon, F. Ricci Lucchi and R.D.A. Smith), pp. 212–215. Chapman & Hall, London.

Kidd, R.B., Lucchi, R.G., Gee, M. and **Woodside, J.M.** (1998) Sedimentary processes in the Stromboli Canyon and Marsili Basin, SE Tyrrhenian Sea: results from side-scan sonar surveys. *Geo-Mar. Lett.*, **18,** 146–154.

Kneller, B.C. and **Branney, M.J.** (1995) Sustained high-density turbidity currents and the deposition of thick massive sands. *Sedimentology*, **42,** 607–616.

Kolla, V., Eittreim, S., Sullivan, L., Kostecki, J.A. and **Burckle, L.H.** (1980) Current-controlled, abyssal microtopography and sedimentation in Mozambique Basin, Southwest Indian Ocean. *Mar. Geol.*, **34,** 171–206.

Komar, P.D. (1971) Hydraulic jumps in turbidity currents. *Geol. Soc. Am. Bull.*, **82,** 1477–1488.

Komar, P.D. (1975) Supercritical flow in turbidity currents: a discussion. *J. Sed. Petrol.*, **45,** 747–749.

Lewis, K.B. (1994) The 1500-km long Hikurangi Channel: trench-axis channel that escapes its trench, crosses a plateau, and feeds a fan drift. *Geo-Mar. Lett.*, **14,** 19–28.

Lewis, K.B., Collot, J.-V. and **Lallemand, S.E.** (1998) The dammed Hikurangi Trough: a channel-fed trench blocked by subducting seamounts and their wake avalanches (New Zealand—France GeodyNZ Project). *Basin Res.*, **10,** 441–468.

Lonsdale, P.F. (1982) Sediment drifts of the Northeast Atlantic and their relationship to the observed abyssal currents. *Bull. Inst. Géol. Bassin Aquitaine*, **31,** 141–150.

Lonsdale, P.F. and **Hollister, C.D.** (1979) A near-bottom traverse of Rockall Trough: hydrographic and geologic inferences. *Oceanol. Acta*, **2,** 91–105.

McCave, I.N. and **Carter, L.** (1997) Recent sedimentation beneath the Deep Western Boundary Current off northern New Zealand. *Deep-Sea Res.*, **44,** 1203–1237.

McCave, I.N. and **Tucholke, B.E.** (1986) Deep-current controlled sedimentation in the western North Atlantic. In: *The Geology of North America*, Vol. M, *the Western North Atlantic Region* (Eds P.R. Vogt and B.E. Tucholke), pp. 1117–1126. Geological Society of America, Boulder, CO.

Malinverno, A., Ryan, W.B.F., Auffret, G.A. and **Pautot, G.** (1988) Sonar images of the path of recent failure events on the continental margin off Nice, France. *Spec. Paper Geol. Soc. Am.*, **229,** 59–75.

Masson, D.G. (1994) Late Quaternary turbidity current pathways to the Madeira Abyssal Plain and some constraints on turbidity current mechanisms. *Basin Res.*, **6,** 17–33.

Middleton, G.V. (1966) Experiments on density and turbidity currents. II. Uniform flow of density currents. *Can. J. Earth Sci.*, **3,** 627–637.

Morris, S.A., Kenyon, N.H., Limonov, A.H. and **Alexander, J.** (1998) Downstream changes of large-scale bedforms in turbidites around the Valencia channel mouth, north-west Mediterranean: implications for palaeoflow reconstruction. *Sedimentology*, **45,** 365–377.

Mulder, T. and **Cochonat, P.** (1996) Classification of offshore mass movements. *J. Sed. Res.*, **66,** 43–57.

Nakajima, T., Satoh, M. and **Okamura, Y.** (1998) Channel-levee complexes, terminal deep-sea fan and sediment wave fields associated with the Toyama Deep-Sea Channel system in the Japan Sea. *Mar. Geol.*, **147,** 25–41.

Normark, W.R. and **Piper, D.J.W.** (1991) Initiation processes and flow evolution of turbidity currents: implications for the depositional record. In: *From Shoreline to Abyss* (Ed. R.H. Osborne), *Soc. Econ. Petrol. Mineral. Spec. Publ.*, **46,** 207–230.

Normark, W.R., Hess, G.R., Stow, D.A.V. and **Bowen, A.J.** (1980) Sediment waves on the Monterey Fan levee: a preliminary physical interpretation. *Mar. Geol.*, **37,** 1–18.

Parker, G., Garcia, M., Fukushima, Y. and **Yu, W.** (1987) Experiments on turbidity currents over an erodible bed. *J. Hydraul. Res.* **25,** 133–147.

Piper, D.J.W. and **Savoye, B.** (1993) Processes of late Quaternary turbidity current flow and deposition on the Var deep-sea fan, north-west Mediterranean Sea. *Sedimentology*, **40,** 557–582.

Piper, D.J.W., Hiscott, R.N. and **Normark, W.R.** (1999) Outcrop-scale acoustic facies analysis and latest Quaternary development of Hueneme and Dume submarine fans, offshore California. *Sedimentology*, **46,** 47–78.

Rona, P.A. (1969) Linear 'lower continental rise hills' off Cape Hatteras. *J. Sed. Petrol.*, **39,** 1132–1141.

Rothwell, R.G., Pearce, T.J. and **Weaver, P.P.E.** (1992) Late Quaternary evolution of the Madeira Abyssal Plain, Canary Basin, NE Atlantic. *Basin Res.*, **4,** 103–131.

Sarnthein, M., Thiede, J., Pflaumann, U., Erlenkeuser, H., Futterer, D., Koopmann, B., Lange, H. and **Seibold, E.** (1982) Atmospheric and oceanic circulation patterns off Northwest Africa during the past 25 million years. In: *Geology of the Northwest African Continental Margin* (Eds U. von Rad, K. Hinz, M. Sarnthein and E. Seibold), pp. 545–604, Springer-Verlag, Berlin.

Saunders, P.M. (1988) Bottom currents near a small hill on the Madeira Abyssal Plain. *J. Phys. Oceanogr.*, **18,** 868–879.

Schrimpf, W. (1986) The influence of the mixing length assumption on calculating suspended sediment transport. In: *River Sedimentation, Vol. III. Proceedings of the Third International Symposium on River Sedimentation* (Ed. by S. Y. Wang, H. W. Shen and L. Z. Ding). School of Engineering, The University of Mississippi, Mississippi, USA.

Shor, A.N., Piper, D.J.W., Hughes Clarke, J. and **Mayer, L.A.** (1990) Giant flute-like scour and other erosional features formed by the 1929 Grand Banks turbidity current. *Sedimentology*, **37,** 631–645.

Stacey, M.W. and **Bowen, A.J.** (1988) The vertical structure of density and turbidity currents: Theory and observation. *J. Geophys. Res.*, **93,** 3528–3542.

Stow, D.A.V. and **Bowen, A.J.** (1980) A physical model for the transport and sorting of fine-grained sediments by turbidity currents. *Sedimentology*, **27,** 31–46.

Stow, D.A.V. and **Lovell, J.P.B.** (1979) Contourites: their recognition in modern and ancient sediments. *Earth Sci. Rev.*, **14,** 251–291.

Stow, D.A.V. and **Tabrez, A.R.** (1998) Hemipelagites: processes, facies and model. In: *Geological Processes on Continental Margins: Sedimentation, Mass-Wasting and Stability* (Eds M.S. Stoker, D. Evans and A. Cramp), *Geol. Soc. London Spec. Publ.*, **129,** 317–337.

Stow, D.A.V., Reading, H.G. and **Collinson, J.C.** (1996) Deep seas. In: *Sedimentary Environments and Facies* (Ed. H.G. Reading), pp. 395–453, Blackwell, Oxford.

Turner, J.S. (1973) *Buoyancy Effects in Fluids*, Cambridge. 368 pp.

Weaver, P.P.E. (1983) An integrated stratigraphy of the upper Quaternary of the King's Trough Flank area, NE Atlantic. *Oceanol. Acta*, **6,** 451–456.

Weaver, P.P.E. (1994) Determination of turbidity current erosional characteristics from reworked coccolith assemblages, Canary Basin, north-east Atlantic. *Sedimentology*, **41,** 1025–1038.

Weaver, P.P.E. and **Kuijpers, A.** (1983) Climatic control of turbidite deposition on the Madeira Abyssal Plain. *Nature*, **306,** 360–363.

Weaver, P.P.E., Jarvis, I., Lebreiro, S.M., Alibes, B., Baraza, J., Howe, R. and **Rothwell, R.G.** (1998) The Neogene turbidite sequence on the Madeira Abyssal Plain – a history of basin filling and early diagenesis. *Proc. ODP Sci. Res.*, **157,** 619–634. College Station, TX (Ocean Drilling Program).

Webb, D.L. (1993) Seabed and sub-seabed mapping using a parametric system. *Hydrogr. J.*, **68,** 5–13.

Wynn, R.B., Masson, D.G., Stow, D.A.V. and **Weaver, P.P.E.** (2000a) Turbidity current sediment waves on the submarine slopes of the western Canary Islands. *Mar. Geol.*, **163,** 185–198.

Wynn, R.B., Masson. D.G., Stow, D.A.V. and **Weaver, P.P.E.** (2000b) The Northwest African slope apron: a modern analogue for deep-water systems with complex seafloor topography. *Mar. Petrol. Geol.*, **17,** 253–265.

Manuscript received 17 September 1999;
revision accepted 18 May 2000.